COMMUNICATIONS IN SCIENCE AND TECHNOLOGY
Homepage: cst.kipmi.or.id

Preparation of Ni/ZSM-5 and Mo/ZSM-5 catalysts for hydrotreating palm oil into biojet fuel

Wega Trisunaryanti*, Karna Wijaya, Aulia Meylida Tazkia

Department of Chemistry, Universitas Gadjah Mada, Yogyakarta 55281, Indonesia

Article history:
Received: 25 May 2024 / Received in revised form: 22 June 2024 / Accepted: 23 June 2024

Abstract

With the increasing demand for fuel for global usage and CO_2 emissions, greener alternatives are needed, especially in biojet fuel production. Catalyst preparation involves the impregnation of Ni and Mo metals into H-ZSM-5 using a dry impregnation method with spray deposition, resulting in Ni/ZSM-5 and Mo/ZSM-5 catalysts. Catalyst characterization utilizes FT-IR, XRD, SAA, SEM-EDX, XRF, and NH_3-TPD instruments. The activity and selectivity tests of the catalysts were conducted in the hydrotreating of palm oil using Ni/ZSM-5 monolayer, Ni/ZSM-5 bilayer, Mo/ZSM-5 monolayer, Mo/ZSM-5 bilayer, as well as Ni/ZSM-5 bottom-layer and Mo/ZSM-5 top-layer arrangements. The result showed double-layer Ni/ZSM-5 as the best catalyst in activity and selectivity in producing biojet fuel fractions with consecutive conversion, selectivity, and yield of 29.71%, 84.76%, and 24.34%, respectively. The layers of catalyst affected the catalytic activity and selectivity, resulting in a higher yield.

Keywords: Biojet fuel; hydrotreating; molybdenum; nickel; palm oil

1. Introduction

Crude oil and its products currently fulfill the majority of the global transportation energy needs (96.7%) with biofuels accounting for 3.0% and renewable electricity for 0.3% [1]. Consequently, the transportation sector contributes to 24% of direct CO_2 emissions from fuel combustion with aviation alone contributing 2% to global CO_2 emissions [2]. Shifting from fossil fuels to biofuels in the aviation sector is potential to reduce CO_2 emissions by up to 68.1% by 2050, promoting energy diversification and socio-economic well-being [3]. The utilization of New and Renewable Energy (NRE) is a top priority for reducing greenhouse gas effects, maintaining energy resilience, and fostering energy independence, given the significant potential of NRE to be a sustainable energy source in future [4]. Biomass, including palm oil, in this case is used for energy conversion into biofuels. Indonesia, contributing approximately 85-90% of the world's total palm oil production, plays a significant role in this [5-6]. Palm oil contains palmitic acid (34.30%), oleic acid (43.96%) and linoleic acid (14.13%) [7]. Vegetable oils, such as palm oil, can be converted into biojet fuel through various processes, including hydroprocessing, hydrotreating, deoxygenation and cracking [8].

In the process of converting palm oil into biojet fuel, the choice of catalyst is crucial. Heterogeneous acid catalysts are widely used in hydrotreating. While metals can act as catalysts without pre-treatment, they have drawbacks such as low thermal stability, small surface area and susceptibility to sintering. Therefore, metal catalysts need to be dispersed on support materials to enhance catalytic activity. Various supports like zeolite H-USY, HY, H-ZSM-5, and H-Beta have been extensively used for hydrocracking, hydrogenation, and isomerization reactions [9]. Research has focused on modifying zeolites into metal-loaded zeolites by loading noble (e.g. Pt, Pd, Ru, Rh) and non-noble (e.g. Co, Ni, Mo, W) metals onto the support. Noble metal catalysts exhibit high catalytic activity but are expensive due to their scarcity [10]. Nickel (Ni) and Molybdenum (Mo) are chosen in view of their partially filled 3d atomic orbitals, creating unpaired electrons that enhance intermediate compound formation, reduce activation energy, and accelerate reaction rates. Ni is also known for easily releasing products from the catalyst surface [11]. Mo has been proven effective in converting vegetable oils into hydrocarbons, particularly in the hydrodeoxygenation reaction, supporting the deoxygenation selectivity of products because of the half-filled *d* orbitals resulting in oxygen atoms protonation. The research on the conversion of palm oil into short hydrocarbon fractions using NiMo/Zeolite catalyst yielded a 36.32wt% yield, 38.05% selectivity, and 84.30wt% conversion [12].

Impregnation is the most common method for modifying

* Corresponding author.
Email: wegats@ugm.ac.id
https://doi.org/10.21924/cst.9.1.2024.1442

metal catalysts. Wet impregnation is more common, effectively dispersing metals through precursor salts. However, conventional wet impregnation is considered ineffective in industry due to time, cost, and waste production. Therefore, this study employed dry impregnation by spraying that is deemed efficient and economical, suitable for large-scale industrial use, allowing control over small particle formation with uniform distribution and reducing solvent usage and catalyst drying time [13].

Catalyst performance is determined not only by its physical and chemical properties but also by operational conditions (temperature, pressure, or contact time) as well as the characteristics and types of catalyst material. Several studies have investigated the catalytic performance of various heterogeneous acid catalysts for hydrotreating, such as the use of commercial catalysts like Ni/ZSM-5 and Mo/ZSM-5 for converting vegetable oils into biojet fuel. Hydrotreating palm oil with Ni/ZSM-5 catalyst in a tubular packed-bed reactor between 300 and 450°C resulted in the highest jet fuel liquid composition yield of 78.73% at 300°C and 10 bar pressure [14]. Jet A-1 comprises long-chain unbranched alkanes (n-alkanes), long-chain branched alkanes (iso-alkanes), cycloalkanes (naphthenes), and aromatic compounds, resulting in hydrocarbons with carbon atom numbers ranging from C_7 to C_{16} [15,16]. Based on previous research, there has been no report on the application of Ni/ZSM-5 and Mo/ZSM-5 catalysts with different catalyst arrangements in the reactor and relatively low operating temperatures (200°C) and atmospheric pressure for the hydrotreating process of palm oil to produce biojet fuel (C_7-C_{16}).

2. Materials and Methods

2.1. Materials

The materials used in this research included palm cooking oil (Hemart brand) from PT. Bina Karya Prima, H-ZSM-5 catalyst (Meiqi Industry & Trade Co., Ltd, Si/Al=50), ammonium heptamolybdate ($(NH_4)_6Mo_7O_{24}.4H_2O$, Sigma-Aldrich, 101182-250G), nickel (II) nitrate hexahydrate ($(Ni(NO_3)_2.6H_2O$, Merck), deionized water from CV. Bima Aksara Nusa), nitrogen gas (N_2) and hydrogen gas (H_2) from PT. Samator Gas.

2.2. Instruments

The instruments utilized in this study included Fourier Transform Infrared Spectroscopy (FTIR, Thermo Scientific Nicolet iS10), X-Ray Diffraction (XRD, Bruker D8 Advance Eco 6510LA), Surface Area Analyzer (SAA, Micromeritics' Gemini VII 2037 Series version 5.03), Scanning Electron Microscope-Energy Dispersive X-Ray (SEM-EDX, JSM6510LA), X-ray Fluorescence (XRF, Rigaku Nex CG II), Temperature Programmed Desorption of Ammonia (NH_3-TPD, Chemisorb 2750 Micromeritrics) and Gas Chromatography-Mass Spectrometry (GC-MS, Shimadzu QP2010S).

2.3. Preparation of Ni/ZSM-5 and Mo/ZSM-5 catalysts

Metal impregnation into H-ZSM-5 was conducted using the dry impregnation method, inspired by the spray application technique [13]. Nickel (Ni) and Molybdenum (Mo) metals, each with a concentration of 6%, were impregnated onto the H-ZSM-5 support using the dry impregnation method through spray application. For the preparation of Ni/ZSM-5 catalyst, the $Ni(NO_3)_2.6H_2O$ precursor solution was employed, while the Mo/ZSM-5 catalyst utilized $(NH_4)_6Mo_7O_{24}\cdot 4H_2O$. A total of 10 g of H-ZSM-5 was weighed, dried in an oven for 1 hour, and then impregnated with $Ni(NO_3)_2.6H_2O$ and $(NH_4)_6Mo_7O_{24}\cdot 4H_2O$ precursor solutions, respectively, dissolved in 9 mL of deionized water. The impregnation was carried out until a paste was formed in a porcelain dish. The catalyst paste was subsequently dried at 110°C for 2 hours and then calcined under N_2 gas flow, followed by a reduction process using H_2 gas. Both calcination and reduction processes were conducted at a flow rate of 20 mL min^{-1} for 3 hours at a temperature of 500°C. The prepared catalysts were labeled as Ni/ZSM-5 and Mo/ZSM-5, and further characterized using FT-IR, XRD, SAA, XRF, SEM-EDX mapping, and NH_3-TPD. The calculation of the required metal weight was performed by referring to the following formula:

$$Mass = \frac{Mr\ precursor}{Metal\ atomic\ coefficient\ x\ Ar\ metal\ atoms} \times C \times m \quad (1)$$

with:

Mr precursor	= relative molecular mass of the precursor
Ar metal atoms	= the relative atomic mass of the metal
C	= metal concentration (%)
m	= H-ZSM-5 support mass (g)

2.4. Hydrotreating palm cooking oil

The hydrotreating process was conducted with a catalyst-to-feed ratio of 1:100 (w/v). Various arrangements of Ni/ZSM-5 and Mo/ZSM-5 were single, double, and a combination (Ni/ZSM-5 on the bottom and Mo/ZSM-5 on the top). The catalyst, in powder form, was placed in the catalyst container within a semi-batch stainless steel reactor with a dual heater in a one-pot system. Hydrotreating was performed using hydrogen gas at a flow rate of 20 mL min^{-1} for 3 hours. The liquid products were separated into two fractions based on temperature ranges: Fraction I (400 – 475°C) and Fraction II (475 – 550°C). The weight of the liquid products was measured, and analysis was conducted using GC-MS. The liquid products from the best-arranged catalysts were further analyzed using FT-IR. The percentage conversion, selectivity, and yield of biojet fuel fraction compounds (hydrocarbon compounds with a carbon atom range of C_7-C_{16}), primary biojet fuel fraction compounds (n-paraffin, iso-paraffin, naphthene, isoalkene, aromatic), non-biojet fuel fraction compounds ($<C_7$ and $>C_{16}$), and oxygenate compounds were calculated using the formulas as described below.

Conversion (%)

$$= \frac{weight\ of\ liquid\ product\ (g)}{oil\ weight\ (g)} \times 100\ \% \quad (2)$$

Biojet fuel Selectivity (%)

$$= \frac{C_7-C_{16}\ GCMS\ area\ fraction(\%)}{total\ GCMS\ area\ (\%)} \times 100\ \% \quad (3)$$

Non-biojet fuel Selectivity (%)

$$= \frac{<C_7 \text{ and } >C_{16} \text{ GCMS area fraction}(\%)}{\text{total GCMS area } (\%)} \times 100\ \% \quad (4)$$

Oxygenate selectivity

$$= 100\% - (\text{Biojet fuel} + \text{non-biojet fuel Selectivity}) \quad (5)$$

$$\text{Yield (wt\%)} = \text{Selectivity (\%)} \times \text{Conversion (\%)} \quad (6)$$

3. Results and Discussion

3.1 Analysis of the chemical composition of palm cooking oil

The composition of palm oil frying oil consists of triglycerides with various fatty acids. The highest peak indicates oleic acid, reaching a retention time of 32.553 with 43.37% GC area. This suggests that oleic acid is the main component in the triglyceride fatty acids of palm oil frying oil. Additionally, other various triglyceride fatty acid components are present, such as palmitic acid, linoleic acid, stearic acid, myristic acid, and elaidic acid with the retention times of 29.244, 32.407, 33.030, 25.087 and 32.649, respectively, and corresponding fatty acid contents of 39.90, 11.47, 3.55, 0.70, and 0.65%. With such a fatty acid composition, the potential of hydrotreating processes on palm oil frying oil lies in producing biojet fuel fraction compounds with a carbon chain range of C_7 to C_{16}. Table 1 presents the composition of palm oil frying oil.

Table 1. Palm cooking oil compositions analysis by using GC-MS

Retention Time	Compound Name	Compound Formula	GC-MS Area (%)
25.087	Myristic Acid	$C_{14}H_{28}O_2$	0.70
29.244	Palmitic Acid	$C_{16}H_{32}O_2$	39.90
32.407	Linoleic Acid	$C_{16}H_{28}O_2$	11.47
32.553	Oleic Acid	$C_{18}H_{34}O_2$	43.37
32.649	Elaidic Acid	$C_{18}H_{34}O_2$	0.65
33.030	Stearic Acid	$C_{18}H_{36}O_2$	3.55

3.2 Infrared spectroscopy analysis of catalysts

The identification of chemical bonds and functional groups of a compound was based on the vibrational absorptions of each bond in the infrared (IR) spectrum with wavelengths ranging from 4000 to 500 cm^{-1}, as depicted in Fig. 1.

Absorption at the wavenumber around 617 cm^{-1} signified the presence of the O-Mo-O bond vibration. A decrease in both area and intensity of the absorption at around 1087 cm^{-1} was observed, attributed to the blocking effect caused by Ni or Mo metal. Absorptions at approximately 802 cm^{-1} and 1084 cm^{-1} indicated symmetric and asymmetric stretching vibrations of Si-O-Si, respectively [17,18]. Another wavelength absorption at around 1225 cm^{-1} indicated stretching vibrations within tetrahedral SiO_4 or AlO_4. The presence of H-ZSM-5 was detected by an absorption at 550 cm^{-1} wavenumbers. This indicates the asymmetric stretching vibration of the pentasilicate H-ZSM-5 or double five-membered ring (d5r) unit [19]. The bending vibrations of the H-O-H group appeared at the absorption peak at the wavelength of 1635 cm^{-1} [20]. The bending vibrations of the O-H hydroxyl group revealed the physical nature of water absorption in H-ZSM-5. At the wavenumber of 3448 cm^{-1}, a broad peak spectrum indicated the stretching vibration of the O-H hydroxyl group [21]. Absorption at the wavenumber around 465 cm^{-1} indicated the presence of T-O (T= Si or Al) bending vibration. Additionally, at the wavelength of 3650 cm^{-1}, there was a vibration of the Al-OH-Si bond [22]. This was associated with the broad absorption band at the wavenumber of 3448 cm^{-1} of the O-H group [21]. These absorption bands were related to hydroxyl groups, specifically the Al-OH-Si group bridging the framework. At approximately 1635 cm^{-1} and 3448 cm^{-1}, the stretching and bending vibrations of water molecules decreased in the Ni/ZSM-5 and Mo/ZSM-5 catalysts. This was attributed to the high-temperature calcination treatment, leading to a reduction in water molecules on the catalyst material's surface. Fig. 1 shows the FT-IR spectra of the catalysts, showing absorption peaks comparable to those of the H-ZSM-5 sample. This indicated that the metal impregnation process does not significantly determine the presence of functional groups on the support.

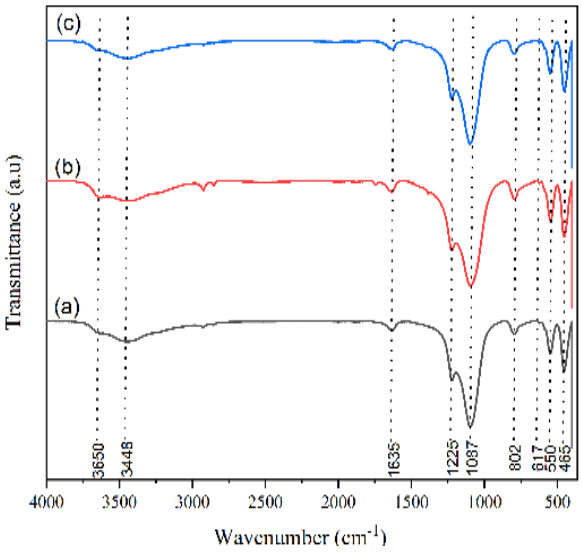

Fig. 1. FT-IR spectra of: a) ZSM-5; (b) Ni/ZSM-5; and (c) Mo/ZSM-5

3.3 Characterization of catalysts by X-ray diffraction

X-Ray Diffraction (XRD) analysis was employed to identify the crystallinity of the catalyst and the presence of metals within it. The compound content in the samples was analyzed by comparing the diffraction angle data and d-spacing values with the International Center for Diffraction Data (ICDD) database. Fig. 2 illustrates the diffractograms of the H-ZSM-5, Ni/ZSM-5, and Mo/ZSM-5 catalysts.

As shown in Fig. 2, the diffractograms of all catalysts were measured in the range of 2θ from 5 to 80°. The XRD analysis results indicated that the consistency of X-ray diffraction peaks with the ICDD database for H-ZSM-5 minerals. Fig. 2 (b) and (c) show that the intensity of H-ZSM-5 peaks decreased with the addition of Ni and Mo metals. However, the crystal structure remained unchanged after loading Ni and Mo onto the surface of H-ZSM-5. The characteristics of H-ZSM-5 peaks (○) were found at 2θ = 8.1°, 8.9°, 14.7°, 23.3°, and 24° (ICDD 00-044-0002), corresponding to the crystal structure of MFI H-ZSM-5. These peaks were used as references to determine the

relative crystallinity of the H-ZSM-5 catalyst. Sharp diffraction peaks indicated good crystallinity [23]. In Fig. 2 (b), several new peaks were observed, indicating the presence of typical Ni metal diffraction peaks (Δ) at 2θ = 44.8°, 52.2°, and 76.8° (ICDD 00-003-1051). This confirmed that NiO has been fully transformed into the Ni form after reduction. Thus, H-ZSM-5 has been impregnated with Ni metal. This is also supported by EDX and XRF analysis as shown in Table 5.

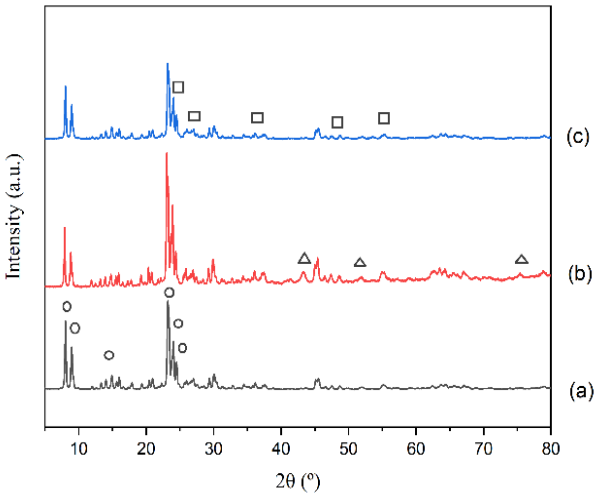

Fig. 2 Diffractogram of: (a) H-ZSM-5 (b) Ni/ZSM-5; and (c) Mo/ZSM-5 catalyst using XRD

In the diffractogram of the Mo/ZSM-5 catalyst in Fig. 2 (c), no peaks of Mo metal were observed. This might be due to the low concentration of Mo metal in the Mo/ZSM-5 catalyst matrix, falling below the detection limit of the XRD instrument. Therefore, to confirm the presence of Mo in the catalyst, XRF and EDX analyses were performed. However, as shown in Fig. 5, typical MoO_3 diffraction peaks (□) appeared at 2θ = 23.7°, 28.7°, 37.1°, 50.5°, and 54.9° (ICDD 01-084-1360). The impregnation process of active metal on the support led to the dispersion of active metal, filling the support pores and forming Mo and Ni oxides during the calcination process. Although the purpose of reducing the catalyst was to produce Mo with an oxidation state of 0, the diffraction results indicated the presence of MoO_3, indicating that the completeness of the reduction process has not been achieved in the Mo/ZSM-5 catalyst [24]. High temperature, gas flow, and extended time were required for this process.

The analysis of the degree of crystallinity for each catalyst sample was conducted by help of Origin Pro software. The relative crystallinity of the catalyst decreased after metal impregnation. The reduction in relative crystallinity was attributed to the coverage of metal species on the catalyst surface, blocking the pores and disrupting the regular structure of the H-ZSM-5 framework. Table 3 presents the results of the degree of crystallinity.

Table 3. Crystallinity of H-ZSM-5; Ni/ZSM-5; and Mo/ZSM-5 catalysts

Catalysts	Crystallinity (%)
H-ZSM-5	76.9
Ni/ZSM-5	68.7
Mo/ZSM-5	71.4

3.4 Catalyst textural characterization by SAA

The reduction in surface area in the Ni/ZSM-5 and Mo/ZSM-5 catalysts was attributed to the impregnation of Ni and Mo metals dispersed across the entire surface of the H-ZSM-5 catalyst. The decrease in catalyst surface area indicated a high metal content covering the catalyst pores [25]. The decrease of pore volume after metal impregnation might be caused by the metal particles agglomerate on the H-ZSM-5 pores as seen in Fig. 5 and Fig. 6. The Mo/ZSM-5 catalyst had smaller pore diameters compared to the H-ZSM-5 catalyst. This was caused by impregnation and calcination, resulting in the closure of the average pore diameter of the catalyst. Mo metal could attach to the pore walls of H-ZSM-5, causing a decrease in pore diameter when the metal adhered to the pore walls. The high metal content in the Ni/ZSM-5 catalyst increased the diameter of the catalyst pores as the metal covered small pores and leaves large pores. The agglomeration of Mo or Ni metals can occur either by attaching to the pore walls or by entering the pores, causing a narrowing of the pore diameter if the metal accumulates on the pore walls and reduces pore volume if the metal settles inside the H-ZSM-5 pores. The increase in pore diameter in the catalyst facilitates easier adsorption, allowing the catalyst to reach its maximum catalytic activity [26]. Table 4 presents the specific surface area data, total pore volume, and average pore diameter.

Table 4. Characteristics of the catalyst from SAA analysis

catalyst	Specific surface area (m^2 g^{-1})	Total pore volume (cm^3 g^{-1})	Average pore diameter (nm)
H-ZSM-5	264.34	1.87	2.81
Ni/ZSM-5	185.49	0.14	2.86
Mo/ZSM-5	258.61	0.18	2.47

The average pore diameter distribution of the H-ZSM-5, Ni/ZSM-5, and Mo/ZSM-5 catalysts fall within the range of 2<d<50 nm, representing the characteristics of mesopores. Fig. 4 presents the average pore diameter distribution of the catalysts.

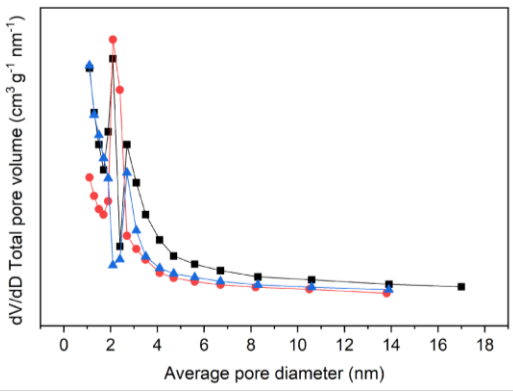

Fig. 4. Average distribution of catalyst pore diameter of: (■) H-ZSM-5; (●) Ni/ZSM-5; dan (▲) Mo/ZSM-5

As shown in Fig. 4, the pore diameter distribution analysis of the H-ZSM-5, Ni/ZSM-5, and Mo/ZSM-5 catalysts revealed that the variance in average pore diameter is observed within the range of 2 to 17 nm with the predominant size concentrated

between 2 and 4 nm. For the Ni/ZSM-5 and Mo/ZSM-5 catalysts, a reduction in distribution intensity was noticeable for pore sizes beyond 6 nm, accompanied by an increase in pore size variation below 6 nm.

3.5 Catalyst morphology and composition characterization by SEM-EDX and XRF

The metal content in the Ni/ZSM-5 and Mo/ZSM-5 catalysts was accurately analyzed using EDX and XRF instruments. The utilization of SEM and mapping techniques on the catalysts aimed to conduct surface morphology analysis with the goal of understanding the morphological structure and metal distribution on the imaged catalyst surface. Characterization using XRF indicated the total metal content throughout the catalyst, while EDX revealed the metal content on the surface of the imaged catalyst. Table 5 presents the results of the elemental composition analysis for the Ni/ZSM-5 and Mo/ZSM-5 catalysts. Theoretically, the Ni/ZSM-5 and Mo/ZSM-5 catalysts were expected to contain 6% of Ni metal for the Ni/ZSM-5 catalyst and 6% of Mo metal for the Mo/ZSM-5 catalyst. The discrepancy between the actual metal content in H-ZSM-5 and the theoretical metal calculation established before the impregnation process indicated suboptimal metal deposition on the support surface during the impregnation process. This could be due to suboptimal preparation of the impregnation solution or catalyst preparation processes, resulting in the uneven dispersion of metals throughout the catalyst or weak interactions between the metal and H-ZSM-5. These factors reduced the amount of active metal on the surface, making the metal more prone to leaching from the catalyst pores.

Table 5. The results of elemental composition analysis in the catalyst using EDX and XRF

Element	EDX (% mass)		XRF (% mass)	
	Ni/ZSM-5	Mo/ZSM-5	Ni/ZSM-5	Mo/ZSM-5
C	10.09	8.46	-	-
O	47.79	5.31	80.50	81,00
Al	2.31	2.36	0.03	0.88
Si	34.11	34.84	15.90	16.90
Ni	5.71	-	2.78	-
Mo	-	4.04	-	1.25

Based on the mapping results as shown in Fig. 5, it can be concluded that the distribution of Mo metal in the Mo/ZSM-5 catalyst on the H-ZSM-5 support is less uniform compared to the distribution of Ni metal in the Ni/ZSM-5 catalyst. This observation was confirmed by the absence of complete coverage by Mo metal across the entire surface of the H-ZSM-5 support. The uneven distribution of Mo metal was attributed to the tendency of Mo metal to agglomerate, leading to non-uniform dispersion and resulting in accumulation at specific points. The coverage of pores by the metal on the support caused a reduction in the surface area [27]. The high content of Ni metal in H-ZSM-5 indicated an increasing amount of metal coating the surface of H-ZSM-5.

The catalyst morphology is corroborated by the SEM results as shown in Fig. 6. Here, the morphology analysis of the Mo/ZSM-5 catalyst revealed a less uniform surface compared to H-ZSM-5 and Ni/ZSM-5. This was characterized by lumps on the Mo/ZSM-5 catalyst. Smaller particles adhered to the lumps were believed to be Ni metal in the Ni/ZSM-5 catalyst and Mo metal in the Mo/ZSM-5 catalyst. This indicated that the addition of metals to the support material determined the morphology of H-ZSM-5, and the metals were successfully impregnated onto H-ZSM-5.

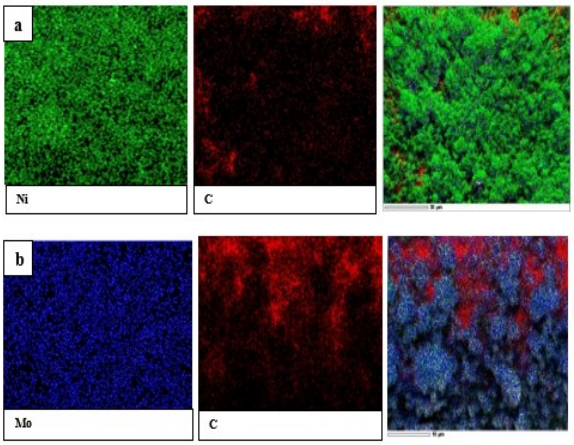

Fig. 5. Image of catalyst mapping (a) Ni/ZSM-5 and (b) Mo/ZSM-5

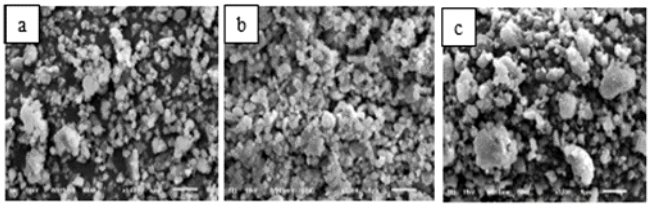

Fig. 6. SEM images of catalysts of: (a) H-ZSM-5; (b) Ni/ZSM-6; and (c) Mo/ZSM-5

3.6 Catalyst acidity using NH_3-TPD

Characterizing acid sites on the catalyst surface involved an analysis using Temperature Programmed Desorption of Ammonia (NH_3-TPD). The total acidity of the catalyst could be revealed through two approaches: extensive factor and intensive factor. The extensive factor reflects the total number of acid sites, while the intensive factor indicates the strength of acid sites present in the catalyst. The classification of acid site strength is divided into weak acid sites, moderate acid sites, and strong acid sites. Weak acid sites are formed at temperatures of 100-350°C, while strong acid sites are formed at temperatures >350°C [28]. As shown in Fig. 7, it can be concluded that the H-ZSM-5, Ni/ZSM-5, and Mo/ZSM-5 catalysts exhibited the peaks of desorption at both weak and strong acid sites. This observation illustrated that metal impregnation contributed to the enhancement of acid site strength in the catalyst, affecting the interaction between the catalyst's active sites and the reactant. Strong acid sites referred to locations with the most intense interaction with the reactant, making it difficult for the reactant to detach from the active catalyst site. Strong acid sites tended to interact with fewer reactants as they were not able to bind to other reactants. Strong acid sites had a moderate level of interaction, allowing interaction with a reactant and releasing the bond after the reaction was completed. On the other hand,

weak acid sites had weaker interactions, making it challenging for the reactant to interact with the catalyst's acid site, resulting in decreased reactivity in those sites. Table 6 detailed the information regarding the acidity profile of the H-ZSM-5, Ni/ZSM-5, and Mo/ZSM-5 catalysts.

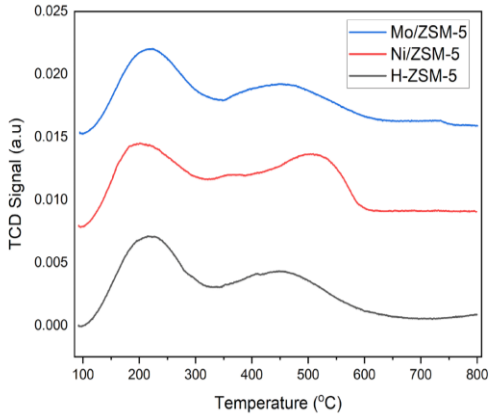

Fig. 7. NH_3-TPD catalyst analysis curve: (—) H-ZSM-5, (—) Ni/ZSM-5, dan (—) Mo/ZSM-5

Table 6. Acidity level of H-ZSM-5, Ni/ZSM-5, and Mo/ZSM-5 catalysts

Acidity (mmol g^{-1})	Catalyst		
	H-ZSM-5	Ni/ZSM-5	Mo/ZSM-5
Weak acid sites	6.52	6.61	6.27
Strong acid sites	2.84	5.69	4.38
Total acidity	9.36	12.30	10.65

Table 6 illustrates an increase in acidity levels after the metal impregnation process. The Ni/ZSM-5 catalyst achieved a maximum acidity of 12.30mmol g^{-1}, while the Mo/ZSM-5 catalyst showed an acidity of 8.27mmol g^{-1}. The Mo/ZSM-5 catalyst exhibited lower acidity compared to Ni/ZSM-5. This could be attributed to the agglomeration of Mo metal on the catalyst's surface, caused by suboptimal metal impregnation. This resulted in the blocking of acid sites on the catalyst due to the presence of metal, leading to the formation of large metal particles or less catalytically active metal phases. The impact of these conditions was evident in the acidity level of the catalyst, where such blockages could hinder or cover existing acid sites on the catalyst. These strong acid sites became highly effective at reaction temperatures ≥ 350°C, facilitating the formation of catalyst-reactant complexes and the production of desired products. The increasing presence of Ni metal successfully impregnated into H-ZSM-5 indicated that Ni also played a role in enhancing the carrier material's acidity, thereby improving the catalyst's acidity. The results from the EDX analysis and mapping images validated these findings.

3.7 Catalyst activity and selectivity test

The main fatty acids in palm oil are oleic acid and palmitic acid. Deoxygenation, decarboxylation, and decarbonylation reactions can only produce hydrocarbons with one carbon shorter than the fatty acids. Therefore, hydrocarbons with bottom carbon numbers are produced by further hydrocarbon cracking reactions into biojet fuel compounds with a carbon chain range of C_7 to C_{16}. Fig. 8 shows the biojet fuel conversion using Ni and Mo catalyst with layer variations results.

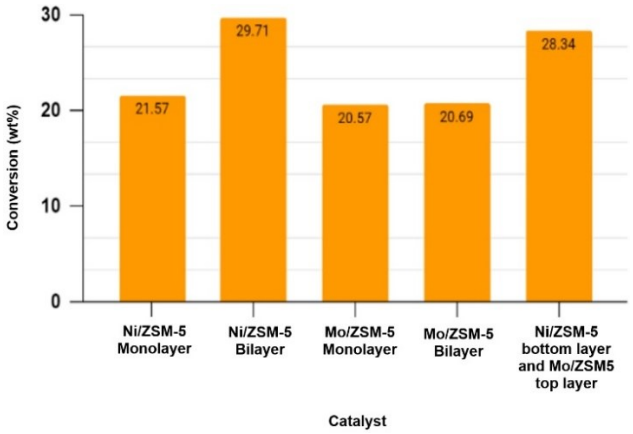

Fig. 8. Palm oil conversion results using: Ni/ZSM-5 monolayer; Ni/ZSM-5 bilayer; Mo/ZSM-5 monolayer; Mo/ZSM-5 bilayer; Ni/ZSM-5 (bottom layer) with Mo/ZSM-5 (top layer)

The utilization of the similar catalyst in two different ranges (bilayer) compared to the similar catalyst in a single range (monolayer) has shown that the bilayer catalyst performed better than the monolayered one. This improvement was attributed to the ability of the bilayer catalyst to optimize the contact area and reaction pressure for each reaction stage. In the first stage of the reaction on the initial catalyst layer, conducted at a bottom pressure, catalyst deactivation in the second reaction stage was minimized. In contrast, the second reaction stage on the second layer was performed at a higher pressure to enhance the quantity and quality of liquid products, thus expediting the formation of liquid products. In a monolayer catalyst within the reactor, the high density of solid catalyst particles reduced the contact area between the catalyst and the reactant. This reduced dispersion of the catalyst diminished active contact with the reactant, resulting in a bottom yield of products. A large contact area allowed the catalyst to interact more thoroughly, accelerating reactions and enhancing selectivity toward products [29]. In the case of a single Ni/ZSM-5 catalyst, it functioned as a hydrocracking catalyst with high hydrogenation activity, breaking down long carbon bonds into shorter molecules. On the other hand, the Mo/ZSM-5 catalyst served as a Hydrodeoxygenation (HDO) catalyst, hydrogenating unsaturated molecules into saturated ones. The Ni/ZSM-5 catalyst performed better than Mo/ZSM-5 catalyst despite having lower surface area as seen in Table 4. The total acidity and Ni content using NH_3-TPD and XRF in Table 5 and 6 showed that Ni/ZSM-5 catalyst had better higher acidity and concentration than Mo/ZSM-5 catalyst. Based on the metal mapping as shown in Fig. 5, Ni was found more evenly spread compared to Mo.

Table 7. Selectivity of liquid products from the hydrotreating process of palm cooking oil based on the analysis of GC-MS results

Catalyst	Selectivity (%)		
	Biojet Fuel	Oxygenated compounds	Non-biojet fuel
Ni/ZSM-5 monolayer	78.95	9.44	11.91
Ni/ZSM-5 bilayer	84.76	8.86	6.14
Mo/ZSM-5 monolayer	78.93	6.31	10.11
Mo/ZSM-5 bilayer	81.82	4.41	11.56
Ni/ZSM-5 bottom layer and Mo/ZSM-5 top layer	83.91	4.70	13.93

Table 8. Liquid products yield composition from the hydrotreating process of palm cooking oil

Catalyst	Yield (%)		
	Biojet Fuel	Oxygenated compounds	Non-biojet fuel
Ni/ZSM-5 monolayer	17.03	2.04	2.57
Ni/ZSM-5 bilayer	24.34	2.54	1.76
Mo/ZSM-5 monolayer	16.32	1.30	2.08
Mo/ZSM-5 bilayer	16.93	0.97	2.39
Ni/ZSM-5 bottom layer and Mo/ZSM-5 top layer	23.78	1.25	3.94

Based on Tables 7 and 8, it was evident that the compound content in the liquid products was resulted from hydrotreating palm oil using monolayered Ni/ZSM-5, bilayer Ni/ZSM-5, monolayered Mo/ZSM-5, bilayer Mo/ZSM-5 catalysts, as well as the bottom-layer Ni/ZSM-5 and top-layer Mo/ZSM-5 catalysts. The H-ZSM-5 did not put into the hydrotreating process due to its ineffectiveness on hydrotreating due to no metal ions contained on the H-ZSM-5, resulting in lower yield as seen in the previous study [30]. The compound content in the liquid products of all catalysts was dominated by compounds within the range of the biojet fuel fraction (C_7-C_{16}). The content of organic compounds and non-biojet fuel hydrocarbon compounds was relatively small, indicating good catalyst selectivity in producing the biojet fuel fraction. The use of bilayer catalysts in the reactor, including both bilayer Ni/ZSM-5 and the bottom-layer Ni/ZSM-5 and top-layer Mo/ZSM-5, exhibited high selectivity in converting palm oil into the biojet fuel fraction compared to the use of monolayered Mo/ZSM-5, whether single or bilayer Ni/ZSM-5. The bilayer catalyst arrangement enhanced catalyst stability, reduced catalyst deactivation due to impurities in the reactor, or products, and improved selectivity for the formation of alkanes and alkenes as the main components of biojet fuel. The bilayer catalyst arrangement in the reactor also optimized catalyst and reactant contact, enhancing the accessibility and diffusion of reactants and products.

The bilayer Ni/ZSM-5 catalyst in the reactor exhibited the highest selectivity and yield for the biojet fuel fraction among all catalyst applications. This was attributed to the good dispersion of Ni metal particles, smaller particle size, large pore diameter, and high total acidity of the Ni/ZSM-5 catalyst. These findings were based on data from SAA, SEM-EDX mapping, XRF, and NH_3-TPD. Therefore, the Ni/ZSM-5 catalyst demonstrated high catalytic activity and selectivity in hydrogen and carbon production. The Ni/ZSM-5 catalyst functions in the cracking process, breaking C-C and C-H bonds in palm oil, resulted in products with higher C_7-C_{16} carbon chains. This aligns research, explaining that the increasing impregnation of Ni metal into H-ZSM-5 leads to more broken C-C and C-H bonds, forming more short-chain products [31].

In the case of the bilayer Mo/ZSM-5 catalyst, it produced fewer organic compounds compared to the top-layer Mo/ZSM-5, bottom-layer Ni/ZSM-5, or top-layer Mo/ZSM-5. This indicated that the Mo/ZSM-5 catalyst removed more oxygen from cracking products, thereby reducing the oxygen content in biojet fuel without significantly affecting the carbon chain length. Therefore, the Mo/ZSM-5 catalyst was more inclined towards high hydrodeoxygenation (HDO) reactions. When using the bottom-layer Ni/ZSM-5 or top-layer Mo/ZSM-5 catalyst, both HDO and hydrocracking reactions became more optimal. Based on Fig. 9, it was evident that the liquid products resulting from hydrotreating with a carbon chain range of C_7 to C_{16} were predominantly hydrocarbons with a carbon chain of C_9-C_{13}. The liquid products from hydrotreating palm oil fell within the carbon number range typical for aviation fuel, specifically C_{13}. This indicated that the prepared catalysts exhibited good selectivity in producing important compounds commonly found in biojet fuel.

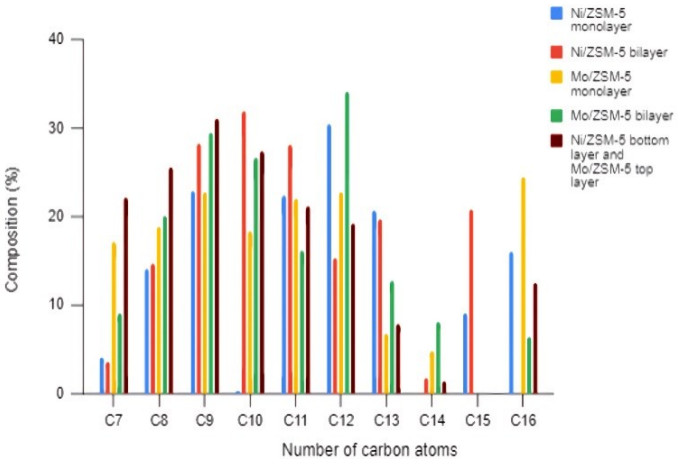

Fig. 9. Carbon atoms distribution from palm cooking oil hydrotreatment with using: Ni/ZSM-5 monolayer; Ni/ZSM-5 bilayer; Mo/ZSM-5 monolayer; Mo/ZSM-5 bilayer; Ni/ZSM-5 (bottom layer) with Mo/ZSM-5 (top layer)

Fig. 10 shows that the biojet fuel fraction contained various compound groups such as paraffins, naphthenes, olefins, cycloalkenes, and aromatics. The main dominance in all liquid products came from the paraffin and olefin groups. This aligned with the research converting biojet fuel products from palm kernel oil (PKO) biomass, showing a composition dominated by paraffin and olefin compound groups [32]. The higher olefin content compared to paraffins in the hydrotreating process of palm oil into biojet fuel indicated that the dehydrogenation reaction was still active in palm oil. Hydrocracking processes also facilitate the formation of olefin compounds through various reaction mechanisms, such as isomerization, dehydrogenation, and molecular cleavage [33].

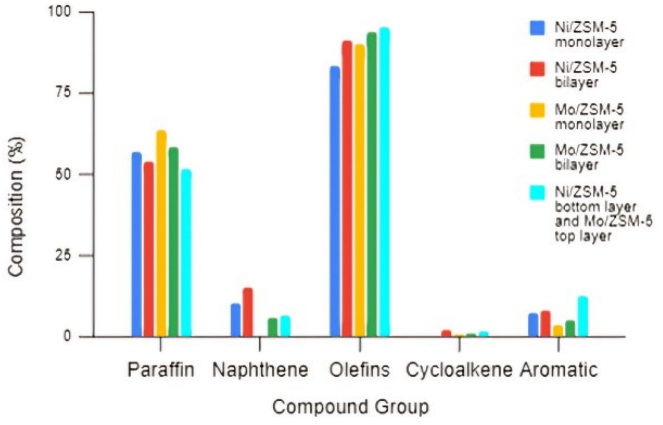

Fig. 10. Biojet fuel fractions in the liquid product obtained from the hydrotreating of palm cooking oil

The highest content of paraffin compounds was observed in the biojet fuel product using the monolayered Mo/ZSM-5 catalyst. Meanwhile, the highest content of naphthenes and cycloalkenes was resulted from the use of the bilayer Ni/ZSM-5 catalyst. Biojet fuel products generated using the bottom-layer Ni/ZSM-5 and top-layer Mo/ZSM-5 catalysts exhibited the highest content of olefin and aromatic compounds. Fig. 10 presents the distribution of hydrocarbon compounds in the liquid product, specifically within the biojet fuel fraction.

3.8. FTIR test analysis of liquid products

FT-IR analysis was conducted to compare the functional groups of palm oil as the main raw material with the hydrotreating product. The spectra of palm oil as the raw material and the liquid product from the hydrotreating process, specifically fractions I and II, using the bilayer Ni/ZSM-5 catalyst, are presented in Fig. 11. Differences were observed in the FT-IR spectra between palm oil and the hydrotreating product, exhibiting significant changes in each type of bond between palm oil and biojet fuel. Hydrocarbon chains were evident in the spectra with varying absorptions due to carbon-carbon bonds. The main absorption in the -CH_2- region, characteristic of alkane absorption, occurred around 3050-2800 cm^{-1} [34]. The increasing trend in alkane compounds indicated the formation of paraffin products in the biofuel. The presence of stretching vibration (C=C) related to alkene or aromatic was indicated by weak absorptions in the 1600-1450 cm^{-1} and 900 cm^{-1} regions [35], suggesting dehydrogenation and aromatization. The appearance of new absorption bands in the 750-720 cm^{-1} region (Fig. 11 (a) and (b)) indicated the possibility of three methylene groups (-CH_2-CH_2-CH_2-CH_2) [34]. Additionally, strong absorption spectra observed between 1320-1100 cm^{-1} and 1800-1700 cm^{-1} also experienced a reduction in absorption in the liquid product from hydrotreating. Bonds in this range corresponded to the stretching vibrations of C-O in alcohol or ether and the stretching vibrations of carboxylate ester groups C=O [34-37]. This drastic reduction indicated the cleavage of C-O bonds in palm oil after hydrotreating.

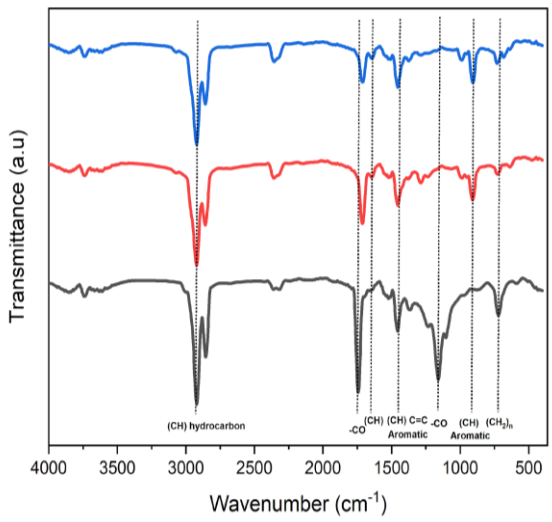

Fig. 11. FT-IR spectra of: (a) palm oil, (b) liquid product of fraction I, and (c) liquid product of fraction II using the dual-layered Ni/ZSM-5 catalyst

Table 9. Comparison of catalyst performance in producing biojet fuel yield based on other studies

Reactant	Reactor	Catalyst	Reaction conditions	Yield (%)	Reference
Palm cooking oil	Semi-batch with double heating	Ni/ZSM-5 bilayer	400°C, 1 atm, H_2 flow rate 20 mL/min	24.34	Present work
Waste cooking oil	Semi-batch	NiCo/SBA-15	350°C, 5 bar	18	[38]
Palm olein	Stainless-steel high-pressure	Ni/modified beta zeolite	340°C, 40 bar	22.1	[39]
Farnesene	Fixed bed	Co-Mo/γ-Al_2O_3	370°C, 60 bar, H_2 flow rate 10 mL/min	20	[40]
Palm olein	Batch	Ni/NH_4-Beta	360 °C, 40 bar	20.8	[41]
Ligno selulosa	Fixed-bed tubular quartz	Cu/Zeolit	300°C, 2 bar, H_2 flow rate 10 mL/min	19	[42]
Palm oil	Fixed bed	NiAg/SAPO-11	360°C, 30 bar, H_2 flow rate 50 mL/min	19	[43]

As seen in Table 9, the current study of palm cooking oil conversion into biojet fuel using a bilayer Ni/ZSM-5 catalyst had a higher yield than previous works. Compared to previous works [38–43] that used higher pressure from 2 to 60 bar, current study used no additional pressure; hence, the current study used less energy. Therefore, the current study has a more efficient performance.

4. Conclusion

The impregnation of Ni or Mo onto the H-ZSM-5 catalyst using the dry impregnation method with spraying resulted in the modification of the characteristic features of the H-ZSM-5 catalyst. After the hydrotreatment of palm cooking oil, double-layer Ni/ZSM-5 was found as the best catalyst based on catalytic activity and selectivity in producing biojet fuel fractions with consecutive conversion, selectivity, and yield of 29.71%, 84.76%, and 24.34%, respectively. Hence, catalyst layers affected the catalyst performance in HDO reaction. The development of improved impregnation methods and reduction processes is essential to minimize Mo oxide content in the catalyst. This ensures the complete reduction of Mo to Mo(0) in future research. Additionally, adjustments in reaction conditions are required to maximize the production of paraffin compounds over olefins in the resulting products.

5. Acknowledgements

Authors thank Universitas Gadjah Mada for financial support under the RTA 2024 project (Contract Number: 4971/UN1.P1/PT.01.01/2024)

References

1. Dhabi: International Renewable Energy Agency, 2023.
2. International Energy Agency (IEA). *Tracking Transport 2020*. France, Paris, 2020.
3. M.D. Staples, R. Malina, P. Suresh, J. I. Hileman and S. R. H. Barrett, *Aviation CO_2 emissions reductions from the use of alternative jet fuels*, Energy Policy 114 (2018) 342-354.
4. B. P. Resosudarmo, J. F. Rezki, and Y. Effendi, Y., *Prospects of Energy Transition in Indonesia*, Bull. Indones. Econ. Stud. 59 (2023) 149-177.
5. Oil World, *Oil World Database*, 2018.
6. S.J. Priatna, Y.M. Hakim, M.A. Alfarizi, S. Sailah, and R. Mohadi, *Palm oil mill effluent (POME) precipitation using ammonium-intercalated clay coagulant*, Commun. Sci. Technol. 8 (2023) 10-15.
7. A.Y. Allam, Z.S. Khan, M.S. Bhat, B. Naik, S.A. Wani, S. Rustagi, T. Aijaz, M.F. Elsadek, and T.W. Chen, *Chemical, Physical, and Technological Characteristics of Palm Olein and Canola Oil Blends*, J. Food Qual. 2023 (2023) 1-17.
8. M. Makcharoen, A. Kaewchada, N. Akkarawatkhoosith, and A. Jaree, *Biojet fuel production via deoxygenation of crude palm kernel oil using Pt/C as catalyst in a continuous fixed bed reactor*, Energy Convers. Manag. X. 12 (2021) 100125.
9. A. Kostyniuk, D. Bajec, A. Prašnikar and B. Likozar, *Catalytic hydrocracking, hydrogenation, and isomerization reactions of model biomass tar over (W/Ni)-zeolites,* J. Ind. Eng. Chem. 101 (2021) 293-306.
10. R. Saab, K. Polychronopoulou, L. Zheng, S. Kumar and A. Schiffer, *Synthesis and performance evaluation of hydrocracking catalysts: A review,* J. Ind. Eng. Chem. 89 (2020) 83-103.
11. N. Panarmasar, N. Hinchiranan and P. Kuchonthara, *Catalytic hydrotreating of palm oil for bio-jet fuel production over Ni supported on mesoporous zeolite,* Materials Today: Proceedings 57 (2022) 1082-1087.
12. M. F., B. H . Carli, Susanto and T. K. Habibie, *Synthesis of bioavture through hydrodeoxygenation and catalytic cracking from oleic acid using NiMo/Zeolit catalyst*, E3S Web of Conferences EDP Sciences 67 (2018) 02023.
13. W. Trisunaryanti, Triyono, K. Wijaya, I. Kartini, S. Purwono, Rodiansono, A. Mara, and A. Budiansyah, *Preparation of Mo-impregnated mordenite catalysts for the conversion of refined kernel palm oil into bioavtur,* Commun. sci. technol., 8 (2023) 226-234.
14. E. Zikhonjwa, *Hydrogenation of coconut oil into Biofuel (bio-jet fuel and high-value low molecule hydrocarbons*, *Doctoral dissertation,* Chemical Engineering, Durban University of Technology, Durban, South Africa, 2021.
15. M. Braun-Unkhoff, T. Kathrotia, B. Rauch and U. Riedel, *About the interaction between composition and performance of alternative jet fuels,* J. CEAS Aeronaut. 7 (2016) 83-94.
16. D. U. Ruixue, L. I. U. Zelong, W. A. N. G. Naixin and L. I. U. Mingxing, *Analysis of Carbon Number Distribution of Hydrocarbons in Jet Fuel by Gas Chromatography-Mass Spectrometry*, Acta Petrolei Sinica (Petroleum Processing Section), 38. 4 (2022) 917-928.
17. A. Aneu, K. Wijaya and A. Syoufian, *Porous Silica Modification with Sulfuric Acids and Potassium Fluorides as Catalysts for Biodiesel Conversion from Waste Cooking Oils*, J. Porous Mater., 29 (2022) 1321–1335.
18. K. Wijaya, W.D. Saputri, I.T.A. Aziz, Wangsa, E. Heraldy, L. Hakim, A. Suseno, and M. Utami, *Mesoporous Silica Preparation Using Sodium Bicarbonate as Template and Application of the Silica for Hydrocracking of Used Cooking Oil into Biofuel,* Silicon 14 (2022) 1583–1591.
19. G.G. Oseke, A. Y. Atta, B. Mukhtar, B. J. El-Yakubu and B. O. Aderemi, *Synergistic effect of Zn with Ni on ZSM-5 as propane aromatization catalyst: effect of temperature and feed flowrate*, J. Porous Mater. 29. 6 (2022) 1839-1852.
20. W. N. A. A. W. Ranizang, S. M. M. Shukri, Z. Y. Zakaria, M. Jusoh and M. A. M. Yussuf, *Catalytic Pyrolysis of Fuel Oil Blended Stock to Methane and Hydrogen Gases Products Using Ni/ZSM-5 catalyst*, Chem. Eng. Trans. 106 (2023) 43-48.
21. K. Wijaya, A. Nadia, A. Dinana, A. F. Pratiwi, A. D. Tikoalu and A. C. Wibowo, *Catalytic Hydrocracking of Fresh and Waste Frying Oil over Ni- and Mo-based Catalysts Supported on Sulfated Silica for Biogasoline Production, Catalysts* 11 (2021) 1150–1164.
22. Y. K. Krisnandi, B.A. Samodro, R. Sihombing and R. F. Howe, *Direct synthesis of methanol BY partial oxidation of methane with oxygen over cobalt modified Mesoporous H-ZSM-5 catalyst*, Indones. J. Chem. (2015) 263-268.
23. Pan, M., Zheng, J., Liu, Y., Ning, W., Tian, H., and Li, R., *Construction and practical application of a novel zeolite catalyst for hierarchically cracking of heavy oil*, J. Catal., 369 (2019) 72–85.
24. T. Riyanto I. Istadi, B. Jongsomjit,D.D. Anggoro, A.A. Pratama and M.A.A. Faris, *Improved Brønsted to Lewis (B/L) Ratio of Co- and Mo-Impregnated ZSM-5 Catalysts for Palm Oil Conversion to Hydrocarbon-Rich Biofuels,* Catalysts 11 (2021) 1286.
25. J. Zhou, J. Zhang, T. Zhang, M. Ye, and Z. Liu, *Regeneration of catalysts deactivated by coke deposition: A review,* Chinese J. Catal., 41. 7 (2020) 1048-1061.
26. S. Chavez B. Werghi, K.M.S. Gutierrez, R. Chen, S. Lall, and M. Cargnello, *Studying, promoting, exploiting, and predicting catalyst dynamics: the next frontier in heterogeneous catalysis*, J. Phys. Chem. C 127. 5 (2023) 2127-2146.
27. P. Kumar, S. K. Maity and D. Shee, *Role of NiMo Alloy and Ni Species in the Performance of NiMo/Alumina Catalysts for Hydrodeoxygenation of Stearic Acid: A Kinetic Study*, ACS Omega 4 (2019) 2833–2843.
28. S.A. Ali, F. M. Almulla, B. R. Jermy, A. M. Aitani , R.H. Abudawoud, M.A. Amer , Z. S. Qureshi, T. Mohammad, and H.S. Alasiri, *Hierarchical composite catalysts of MCM-41 on zeolite Beta for conversion of heavy reformate to xylenes*, J Ind Eng Chem. 98 (2021) 189-199.
29. Z. Hu, P. Hu , X. Wang , T. Wu , S. Ge , H. Xie , B. Liu , S. Chen , and Z. Wu, *Selective hydrocracking of 1-methylnaphthalene to benzene/toluene/xylenes (BTX) over NiW/Beta bifunctional catalyst: Effects of metal–acid balance*, Fuel 363 (2024) 130947.
30. W. Trisunaryanti, K. Wijaya, I. Kartini, S. Purwono, Rodiansono, A. Mara, A. S. Rahma, *Hydrodeoxygenation of refined palm kernel oil (RPKO) into bio-jet fuel using Mo/H-ZSM-5 catalysts*, React. Kinet. Mech. Catal. 137 (2024) 843-878.
31. Q. L. Li, R. Shan, J. Zhang, M. Lei, H. R. Yuan and Y. Chen, *Enhancement of hydrogen and carbon nanotubes production from hierarchical Ni/ZSM-5 catalyzed polyethylene pyrolysis*. J. Anal. Appl. Pyrolysis 169 (2023) 105829.
32. E. S. S. Why, H. C. Ong, H. V. Lee, W. H. Chen, N. A. Mijan and M. Varman, *Conversion of bio-jet fuel from palm kernel oil and its blending effect with jet A-1 fuel*, Energy Convers. Manag., 243 (2021) 114311.
33. F. S. AlHumaidan, R. Bouresli, H. AlSheeha, M. Marafi and M. S. Rana, *Synthesis of Mild Hydrocracking Catalysts for Residue Conversion,* Ind. Eng. Chem. Res. 63.1 (2023) 100-110.
34. E. Fumoto, S. Sato and T. Toshimasa, *Determination of carbonyl functional groups in heavy oil using infrared spectroscopy*, Energy Fuels 34. 5 (2020) 5231-5235.
35. L. D. R. Novaes, A. R. Secchi, V. M. M. Salim and N. S. de Resende, *Enhancement of hydrotreating process evaluation: correlation between feedstock properties, in-line monitoring and catalyst deactivation*, Catal. Today 394 (2022) 390-402.
36. H. Hafshah, D. H. Prajitno and A. Roesyadi, *Hydrotalcite Catalyst for Hydrocracking Calophyllum inophyllum Oil to Biofuel: A Comparative Study with and without Nickel Impregnation,* Bull. Chem. React. Eng. Catal. 12. 2 (2017) 273-280.
37. M. Anand, S. A. Farooqui, J. Singh, H. Singh and A. K Sinha, *Mechanistic in-operando FT-IR studies for hydroprocessing of triglycerides*, Catal. Today 309 (2018) 11-17.
38. D. Banerjee, I.S. Yunus, X. Wang, J. Kim, A. Srinivasan, R. Menchavez, Y. Chen, J.W. Gin, C.J. Petzold, H.G. Martin, J.K. Magnuson, P.D. Adams, B.A. Simmons, A. Mukhopadhyay, J. Kim, and T.S. Lee, *Genome-scale and pathway engineering for the sustainable aviation fuel precursor isoprenol production in Pseudomonas putida,* Metab. Eng. 82 (2024) 157-170.
39. N. Hunsiri, N. Chaihad, C. Ngamcharussrivichai, D.N. Tungasmita, P. Reubroycharoen, and N. Hinchiranan, *Branched-chain biofuels derived from hydroisomerization of palm olein using Ni/modified beta zeolite catalysts for biojet fuel production,* Fuel Process. Technol. 248 (2023) 107825.
40. A. Tepelus, R.E Dragomir and P. Rosca, *Biojet from Sugar Derivatives*, Rev. Roum. Chim. 66. 4 (2021) 313-320.
41. P. Chintakanan, T. Vitidsant, P. Reubroycharoen , P. Kuchonthara, T. Kida, N. Hinchiranan, *Bio-jet fuel range in biofuels derived from hydroconversion of palm olein over Ni/zeolite catalysts and freezing point of biofuels/Jet A-1 blends,* Fuel 293 (2021) 120472.
42. S. P. Adhikari, J. Zhang, Q. Guo, K.A. Unocic, L. Tao and Z. Li, *A hybrid pathway to biojet fuel via 2, 3-butanediol*, Sustain. Energy Fuels, 4. 8 (2020) 3904-3914.
43. C.H. Lin, Y.K. Chen and W.C Wang, *The production of bio-jet fuel from palm oil derived alkanes,* Fuel 260 (2020) 116345.